CHEMISTRY OF MATERIALS

Article

pubs.acs.org/cm

Cooperative Assembly of Hydrogen-Bonded Diblock Copolythiophene/Fullerene Blends for Photovoltaic Devices with Well-Defined Morphologies and Enhanced Stability

Ying Lin,[†] Jung Ah Lim,[†] Qingshuo Wei,[†] Stefan C. B. Mannsfeld,[‡] Alejandro L. Briseno,[†] and James J. Watkins*,[†]

[†]Department of Polymer Science and Engineering, University of Massachusetts Amherst, 120 Governors Drive, Amherst, Massachusetts 01003

[‡]Stanford Synchrotron Radiation Lightsource, 2575 Sand Hill Road, Menlo Park, California 94025

Supporting Information

ABSTRACT: We report the cooperative self-assembly of functionalized fullerenes and all conjugated block copolymers (BCPs) containing polythiophene derivatives in both segments to yield solar cells with well-defined nanostructures and enhanced morphological stability. Favorable hydrogen bonding interactions between the COOH-functionalized fullerene, bis-[6, 6]-phenyl C61-butyric acid (bis-PCBA), and the tetraethyleneglycol side chains of poly(3-hexylthiophene)-*block*-poly[3-(2,5,8,11-tetraoxadodecane)thiophene] (P3HT-*b*-P3TODT) allows for high loading of bis-PCBA (up to 40 wt % to the blend) within the P3TODT domains, while preserving the lamellar morphology. Characterization by grazing incidence small-angle X-ray scattering, electron microscopy, and atomic force microscopy indicates that the periods of the structures range between 24 and 29 nm depending on the bis-PCBA loading. The hydrogen bond interactions between bis-PCBA and P3TODT segments further suppress crystallization and macrophase separation of the fullerenes, even under harsh annealing conditions (150 °C for 12 h). Bulk heterojunction solar cells prepared using P3HT-*b*-P3TODT/bis-PCBA exhibit a photoconversion efficiency of 2.04%, which is greater than that of a reference system, P3HT-*b*-P3TODT/bis-PCBM. Accelerated aging experiments reveal enhanced thermal stability as a result of the limited translational mobility of COOH-functionalized fullerene in P3HT-*b*-P3TODT relative to devices prepared using bis-PCBM in P3HT-*b*-P3TODT or P3HT. We believe that cooperative assembly using strong noncovalent interactions is a general approach that can be used to improve the processing, morphological stability, and aging of organic and hybrid photovoltaic devices.

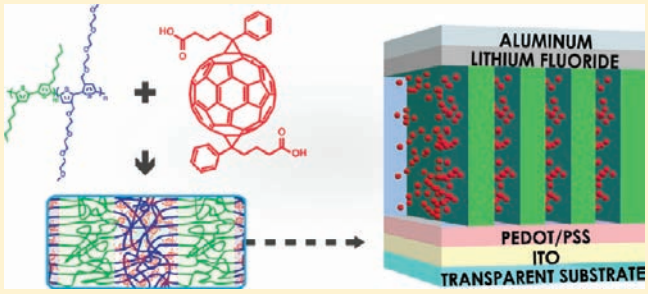

KEYWORDS: *diblock copolymer, self-assembly, morphology, photovoltaic device, hydrogen bonding, supramolecular assembly*

INTRODUCTION

Organic photovoltaics (OPV) have been studied for nearly two decades as a result of the growing interest in renewable energy technologies combined with the need for flexible, low-cost, and large-area processing for economically viable manufacturing.[1−3] One of the most promising OPV devices is based on bulk heterojunction (BHJ) thin films consisting of poly(3-hexylthiophene) (P3HT), an electron-donating polymer, and [6,6]-phenyl-C61-butyric acid methyl ester (PCBM), which serves as an electron acceptor. While extensive efforts to optimize processing conditions have led to power conversion efficiencies (PCE) of approximately 5%, the performance for P3HT/PCBM devices has been stalled near this value for the past few years.[4,5]

Challenges for the preparation of organic BHJ cells include controlling the nanoscale morphology of the components[6,7] and ensuring stability of the desired morphology over the lifetime of the device.[8−12] Because of the limited exciton diffusion length of the organic materials (ca. 10 nm),[3,13,14] organic solar cells require a high interfacial area arrangement of an electron donor and acceptor domains in thin films to achieve efficient charge separation. With respect to these challenges, P3HT/PCBM devices suffer from two specific limitations. First, the domain size and architecture of the heterojunction are not well controlled. The morphology of the donor and acceptor domains are strongly dependent on the processing conditions and can be heavily influenced by P3HT crystallization.[15] Even though the resulting morphologies can be controlled to some extent by process optimization involving controlled thermal annealing,[16,17] solvent annealing,[18] additives,[19] and slow drying of spin-coated films,[20] there are limitations to the size scale and organization of structures that can be obtained by this

Received: December 11, 2011
Revised: January 17, 2012
Published: January 18, 2012

Scheme 1. Chemical Structures of P3HT-*b*-P3TODT and bis-PCBA and Schematic of the Ordered, Self-Assembled Blend that Serves as the Active Layer in the OPV Device

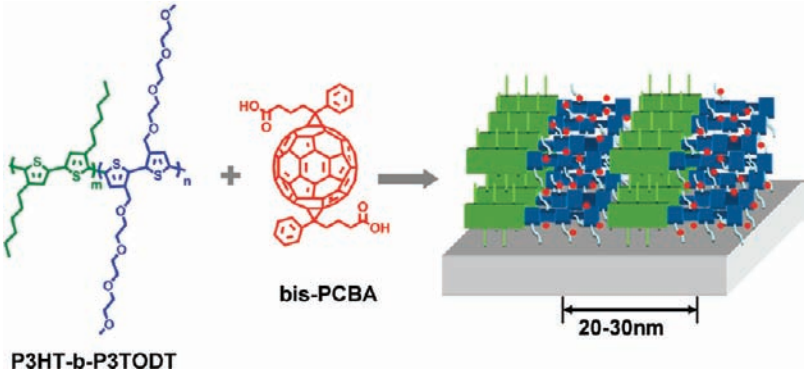

approach. Second, the morphologies achieved by mixing are generally not thermodynamically stable but are nonequilibrium states. This leads to the deterioration of device performance at typical fabrication temperatures and during extended use. Specifically, macrophase separation of blend components can occur upon postprocessing and extended device operation, and as a result, there are significant changes to the as-deposited thin film morphology. Additional instability can arise from diffusion of PCBM during device preparation and use, which results in concentration gradients, depletion from active areas of the device, and in some cases aggregation or crystallization of PCBM.[8,9] PCBM aggregation causes a reduction in the interfacial area available for charge separation and thus impairs device performance. For example, thermal annealing of P3HT/PCBM at 150 °C for over 3 h induces the formation of large aggregates of PCBM, tens of micrometers in length, and as a result, the device performance decreased from 2.5% PCE to 0.5%.[10] Thus, it is desirable to find methods for controlling morphology development to yield efficient charge separation and achieve a stable morphology.

Block copolymers (BCPs) comprised of two or more chemically distinct polymer segments covalently bound at one or more junction points can microphase separate into well-ordered spherical, cylindrical, or lamellar morphologies that are thermodynamically stable and exhibit periodicities from 5 to 50 nm.[21,22] In principle, well-defined cylindrical and lamellar morphologies are particularly attractive for BHJ devices, as domain sizes are commensurate with exciton diffusion lengths, and the morphologies offer the potential for continuous charge conduction pathways. Consequently, block copolymers are of emerging interest as a promising class of materials or templates for PV applications, and comprehensive reviews are available.[23−27] Rod−coil block copolymers containing P3HT as electron donor and companion blocks, such as polystyrene, poly(2-vinyl pyridine), or polylactide have been prepared and studied extensively.[28−30] While the existing literature is contradictory, several works claim that BCPs containing P3HT block form vertical lamellae morphology via microphase separation[28,30] or exhibit the full range of spherical, cylindrical, or lamellar morphologies typical of diblock copolymers.[29] There are, however, other papers that suggest that the morphology of BCPs containing P3HT segments of high molecular weight are dominated by crystallization of the P3HT block. The segment crystallization can frustrate organization of the domains driven by segment microphase separation.[31,32] In addition, P3HT or poly(*p*-phenylenevinylene) (PPV) containing BCPs with covalently linked fullerene moieties or perylenediimide derivatives as electron acceptor have been investigated.[33−36] These single-component systems have potential advantages that include suppression of fullerene aggregation. In this arrangement, however, the fullerene is primarily incorporated within an insulating polymer matrix, which challenges the charge transport properties of the device, and their efficient utilization as the active layer in PVs has not yet been fully demonstrated. Furthermore, the synthesis of block copolymers containing high concentrations of covalently bound fullerene groups is challenging and tedious and therefore difficult to employ at large scales. Recent work reported a diblock co-polythiophene, in which one block carried fullerene.[37] Although well-defined lamellar morphology was not observed, very stable morphology and device performance upon thermal annealing was demonstrated.

Another approach is to use all conjugated block copolymers blended with fullerene derivatives. Advances in synthetic techniques, specifically Grignard metathesis (GRIM) polymerization enables the preparation of regioregular aromatic rod−rod block copolymers with narrow polydispersities,[38,39] although, to date, only a few examples have been reported.[40−45] Tajima and co-workers reported microphase-separation of poly(3-hexylthiophene-block-3-(2-ethylhexyl) thiophene)s (P(3HT-*b*-3EHT)s) upon thermal treatment,[42,43] though no devices have been built to evaluate the influence of morphology on performance.

Here, we report the cooperative self-assembly of functionalized fullerenes and all conjugated diblock copolymers containing polythiophene derivatives in both segments using hydrogen bond interactions between the fullerene and one segment of the BCP (Scheme 1). More specifically, we synthesized diblock copolymers comprised of poly(3-hexylthiophene) and poly[3-(2,5,8,11-tetraoxadodecane)thiophene (P3TODT) and blended them with bis-[6,6]-phenyl-C61-butyric acid (bis-PCBA) to form BHJs. The use of strong interactions between the acid functionality of the fullerene derivative, which serves as a hydrogen bond donor, and oligo(ethylene oxide) within the P3TODT segments accomplishes a number of important goals for BHJ fabrication. These include providing control of the distribution, loading, and physical mobility of the functionalized fullerene at high additive loadings. This approach builds on our reports[46] of the use of segment-specific hydrogen bond interactions between functionalized nanoparticles and block copolymers to prepare well-ordered hybrid materials at high additive loadings. Well-ordered

dx.doi.org/10.1021/cm203706h | *Chem. Mater.* 2012, 24, 622−632

BCP/PCBM blends were reported by the Hadziioannou group, using a supramolecular route based on noncovalent bonds between poly(3-hexylthiophene)-block-poly(4-vinylpyridine) rod−coil block copolymer and PCBM.[47] The use of polythiophene derivatives in both BCP segments as reported here avoids the undesirable use of insulating polymer segments in the device design.

It has been appreciated that hydrogen-bonding encourages better molecular level ordering, enhances molecular rigidity, promotes interfacial electron transfer, improve charge transport, reduces charge trap sites, and extends device lifetime.[48−53] Herein, the utilization of hydrogen-bonding demonstrates a new way to form electron acceptor domains within a block copolymer self-assembled nanostructure. In this paper, we emphasize the morphology of the P3HT-*b*-P3TODT/bis-PCBA blends, and its relationship to device properties. It is shown that the addition of the functionalized C60 increases segregation of the donor and acceptor domains. The thermal stability of the devices prepared using this approach is dramatically improved in comparison to devices based on P3HT/PCBM blends.

EXPERIMENTAL SECTION

Materials. Bis-PCBA was synthesized by standard acid hydrolysis from bis-PCBM (99.5%, Nano-C Inc.). The 2,5-dibromo-3-alkoxythiophene was synthesized by a modified literature method.[54] 2,5-dibromo-3-hexylthiophene, isopropylmagnesium chloride lithium chloride complex (i-PrMgCl·LiCl, 1.3 M solution in THF), and N-bromosuccinimide (NBS) were purchased from Sigma-Aldrich. Poly(3,4-ethylenedioxy thiophene):poly(styrene sulfonate) (PEDOT:PSS) (Baytron PVP AI 4083) was purchased from HC Stark and passed through a 0.45 μm PES syringe filter before spin-coating. Anhydrous THF was distilled from sodium-benzophenone. Anhydrous chlorobenzene was purchased from sigma Aldrich and used without purification. All other reagents were used as received, unless otherwise stated.

Synthesis of P3HT-*b*-P3TODT block copolymer. The polythiophene block containing oligo(oxyethylene) side chains is designated as P3TODT. The molar feed ratio of **M1** and **M2** was 1:1. The molecular weight was controlled by fixing the ratio of the amount of Ni catalyst to the total monomer amount at 1:100. The typical synthesis procedure of diblock copolymer was as follows: two round-bottomed flasks (100 mL) equipped with a three-neck stopcock were flame-dried and cooled to room temperature. 2,5-Dibromo-3-hexylthiophene (0.978 g, 3.0 mmol) was placed in one flask under N_2, and then evacuated under reduced pressure to remove any moisture and oxygen inside. After anhydrous THF (45 mL) was added into the flask via a syringe, the solution was stirred at 0 °C. 1.3 M solution of i-PrMgCl·LiCl in THF (2.3 mL, 3.0 mmol) was added via a syringe, and the mixture was stirred at 0 °C for 2 h (solution 1). In the other flask, **M2** (1.302 g, 3.0 mmol) was first reacted with i-PrMgCl·LiCl in THF (2.3 mL, 3.0 mmol) (solution 2) at 0 °C for 2 h and then warmed to room temperature. Solution 1 was warmed to room temperature, and Ni(dppe)Cl_2 (31.7 mg, 0.06 mmol) was added in one portion. After stirring for 30 min, solution 2 was transferred to solution 1 via a double-tipped needle, and the resulting solution was stirred at room temperature overnight. The reaction was quenched by adding HCl solution (20 wt %) into the solution. The crude polymer was successively washed by Soxhlet extraction using methanol, hexane, and chloroform. The solvent was removed by evaporation to give a purple solid (0.82 g, yield: 63%).

Solar Cell Device Fabrication and Characterization. Blend solutions were prepared by dissolving polythiophenes/fullerene derivative in different ratios in chlorobenzene at a total concentration of 2 wt %. The solutions were stirred for 12 h before device fabrication. The photovoltaic devices were fabricated according to the following procedure: ITO-coated glass was cleaned with detergent followed by ultrasonication in water, acetone, and isopropyl alcohol, and then was kept at 150 °C for 30 min. After complete drying, ITO-coated glass was treated with UV-ozone to improve the wettability of PEDOT:PSS. After spin-coating 35 nm of PEDOT:PSS, the active layer was spin-coated on top of the PEDOT:PSS layer at 1500 rpm for 60 s. LiF (1 nm) and Al (100 nm) were thermally evaporated under vacuum lower than 3×10^{-6} Torr on the top of the active layer through a shadow mask. For thermal annealing, the completed devices were placed directly onto a digitally controlled hot plate and heated to 150 °C for the desired time. All current−voltage (I−V) characteristics of the devices were measured under simulated AM1.5G irradiation (100 mW cm^{-2}) using a Xe lamp-based Newport 91160 300-W solar simulator. The light intensity was adjusted with an NREL-calibrated Si solar cell with a KG-5 filter. The results reported represent the median of five sets of devices.

Transistor Device Fabrication and Characterization. Top-contact and bottom-gate geometry was used to fabricate and test field-effect transistors prepared using the copolymers. Heavily n-doped silicon substrates acted as gate electrode, and thermally grown silicon dioxide (300 nm thick; C_i = 10.7 nF/cm^2) acted as gate insulator. Octadecyltrichlorosilane (OTS)-modified SiO_2 was prepared by soaking the substrates in a 5 mM toluene solution of OTS for 12 h in a dry N_2-filled glovebox. Substrates with the structure of glass/PSS/P3HT-*b*-P3TODT were prepared by successive spin-coating of an aqueous solution of PSS and a 2 mg/mL chlorobenzene solution of the copolymer. This polymer film was gently brought into contact with the target substrate, with the polymer face down. One drop of water was placed on the edge of the two stacked substrates. The PSS layer was selectively permeated by water. After 1−5 min, the water flowed from one side of the substrate to the other, and the PSS layer was completely dissolved. Finally, the glass substrate was easily detached from the organic layer, resulting in the transfer of the polymer film from the glass to the target substrate. Gold electrodes were evaporated onto the surface through a metal mask with a channel width (W) of 500 μm and length (L) of 50 μm.

Output (I_{ds} vs V_{ds}) and transfer (I_{ds} vs V_g) characteristics of the devices were measured on a Keithley 4200 semiconductor characterization system (Keithley Instruments, Cleveland, OH). Field-effect mobility was calculated from the standard equation for saturation region: $I_{ds} = \mu(W/2L)C_i(V_g - V_t)^2$ where I_{ds} is drain-source current, μ is field-effect mobility, W and L are the channel width and length, C_i is the capacitance per unit area of the gate insulator (C_i = 10.7 nF/cm^2), V_g is the gate voltage, and V_t is the threshold voltage.

Characterization of Morphology. *TEM.* The protocol for preparing the thin films is the same as that for device fabrication. For analysis of the films by transmission electron microscopy (TEM), the specimens were scored and immersed in water to promote dissolution of the PEDOT:PSS layer. The delaminated film was then floated onto a copper TEM grid. TEM was performed on films using a JEOL 2000 CX microscope operating at 200 kV.

AFM. The films for atomic force microscopy (AFM) imaging of surface morphology were spin-coated onto a silicon wafer and annealed at 150 °C for 30 min in a vacuum oven. Tapping-mode AFM was performed with Nanoscope III (Digital Instruments, Inc.).

GISAXS. Grazing incidence small-angle X-ray scattering (GISAXS) experiments were performed at D1 station of the Cornell High Energy Synchrotron Source (CHESS). The wavelength of X-rays used was 1.55 Å, and the angle of incidence was chosen to be above the critical angle of the film under study, to make sure that the collected scattered radiation is the representation of the entire film thickness. The scattered radiation was collected with a two-dimensional charge-coupled device (CCD) camera with image sizes of 1024 pixels by 1024 pixels.

GIXRD. GIXRD measurements were carried out at the Stanford Synchrotron Radiation Lightsource (SSRL) on beamline 11−3 with a photon energy of 12.73 keV. The incidence angle α of the incident beam was set to 0.1#°. The diffraction intensity was detected on a 2D image plate (MAR-345). The distance L = 402 mm between sample and detector was calibrated using a LaB_6 polycrystalline standard.

Scheme 2. (a) Synthetic Route to P3HT-*b*-P3TODT Block Copolymer. (b) GPC Profiles of the Parent P3HT Homopolymer and the Block Copolymer P3HT-*b*-P3TODT

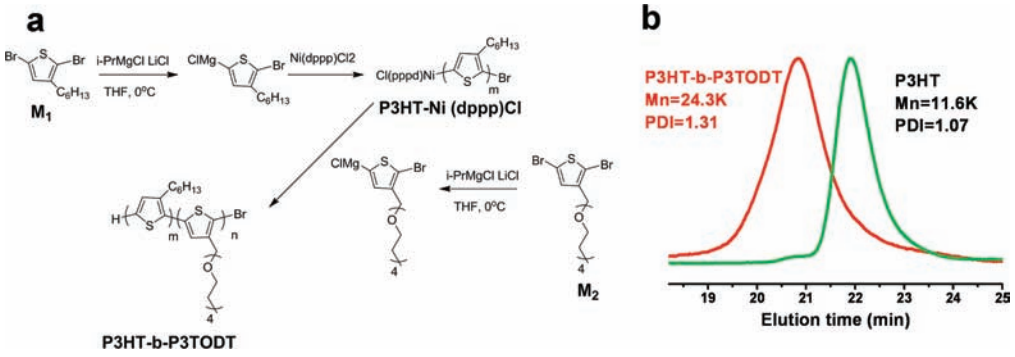

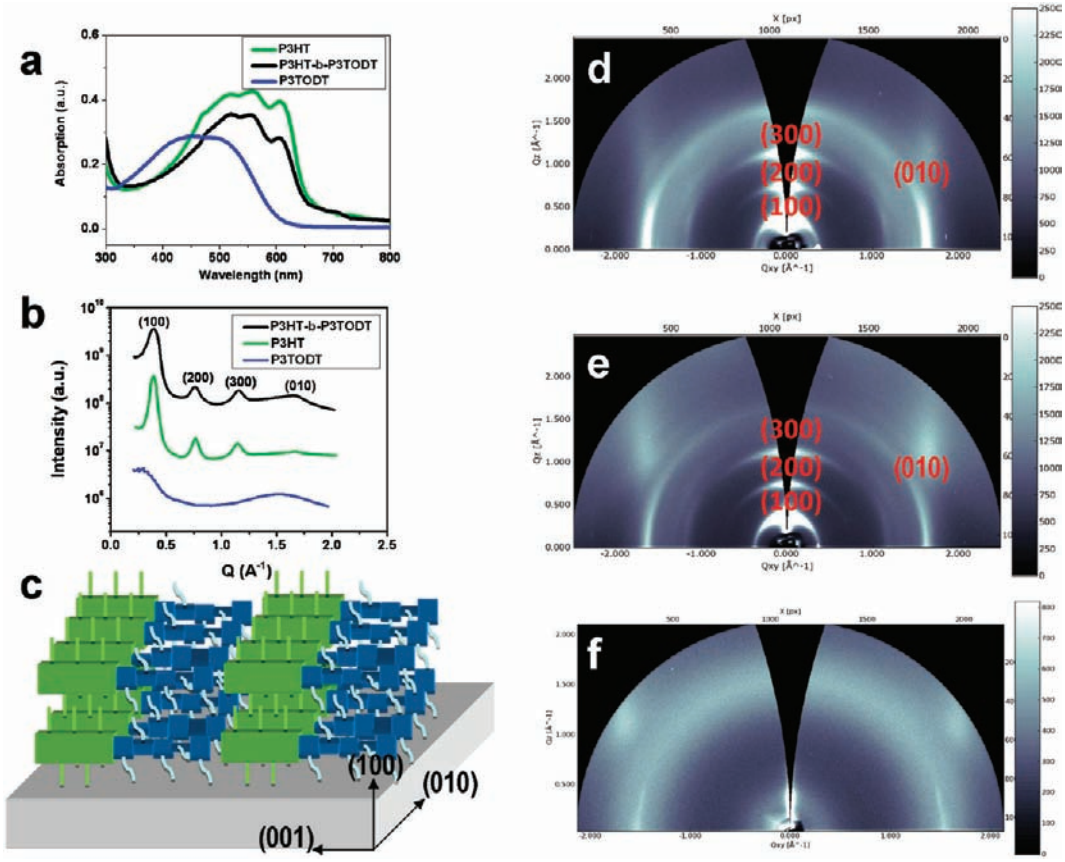

Figure 1. (a) UV−vis absorbance spectra of thin films of P3HT, P3TODT, and P3HT-*b*-P3TODT; (b) overlay of GIXRD out-of-plane diffractograms of all three samples; (c) schematic representation of the proposed film structure of P3HT-*b*-P3TODT after thermal annealing; 2D GIXRD images of (d) P3HT-*b*-P3TODT, (e) P3HT, and (f) P3TODT films after annealing at 150 °C for 30 min.

Reconstruction of out-of-plane scattering profiles from GIXD images and GIXD image analysis was performed with the software WxDiff.[55]

RESULTS AND DISCUSSION

Synthesis and Characterization of Block Copolymer P3HT-*b*-P3TODT. The P3HT-*b*-P3TODT block copolymer was synthesized following the procedure of Yokozawa and co-workers using a modified GRIM method (Scheme 2a).[54] Briefly, the P3HT block was prepared using Ni-catalyzed quasi-living polymerization of 2,5-dibromo-3-hexylthiophene (**M1**), followed by the addition of activated monomer 2 (**M2**) solution. A molar feed ratio of **M1** to **M2** of 1:1 was selected to obtain a lamellar morphology. The actual compositions of two blocks were determined to be 45:55 (P3HT:P3TODT) by weight using ^{1}H NMR (Figure S1 in the Supporting Information). Gel permeation chromatography (GPC) profiles of the P3HT living polymer and P3HT-*b*-P3TODT are shown in Scheme 2b. The number-average molecular weight (M_n) of the block copolymer was 24300 g/mol with a polydispersity index (PDI) of 1.31. The block copolymer exhibits good solubility in $CHCl_3$, CH_2Cl_2, THF, DMF, and cholorobenzene. P3HT and P3TODT homopolymers with molecular weights equivalent to the corresponding blocks in the BCP were synthesized for comparison.

UV−visible absorption spectra of P3HT-*b*-P3TODT, P3HT and P3TODT thin films are shown in Figure 1a. The P3HT-*b*-

dx.doi.org/10.1021/cm203706h | *Chem. Mater.* 2012, 24, 622−632

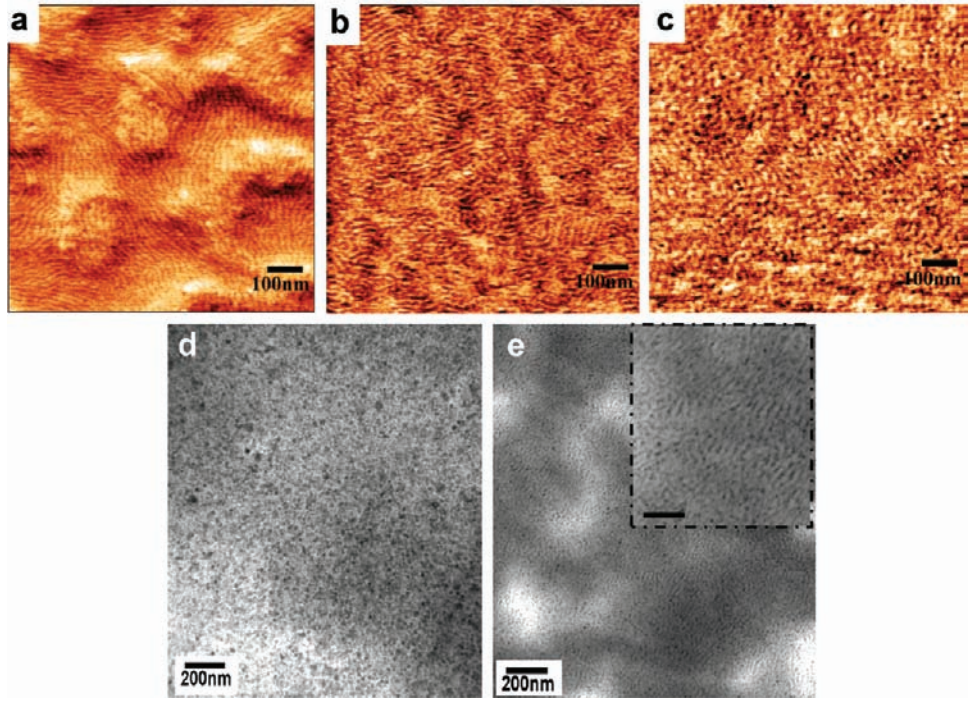

Figure 2. Tapping mode AFM phase images of thin films of (a) P3HT-*b*-P3TODT, (b) P3HT-*b*-P3TODT/bis-PCBA (8/2), and (c) P3HT-*b*-P3TODT/bis-PCBA (6/4), after thermal annealing at 150 °C for 30 min; TEM images of (d) P3HT-*b*-P3TODT/bis-PCBM (3/2) and (e) P3HT-*b*-P3TODT/bis-PCBA (3/2), after thermal annealing at 150 °C for 30 min. The inset in (e) shows an expanded view (scale bar is 100 nm).

P3TODT film exhibits three characteristic peaks at 492, 560, and 610 nm, which are due to the P3HT homopolymer. The absorption shoulder at 610 nm has been reported to be indicative of the strong intermolecular $\pi-\pi$ interaction and suggests a high degree of crystallinity in P3HT homopolymer.[56] In the block copolymer, this peak will arise from the crystalline P3HT segment only (55% by volume), while the weaker shoulder at 610 nm may be attributable to the presence of the noncrystalline P3TODT. The absorbance spectrum of the P3TODT film exhibits a blue shift, as compared to P3HT homopolymer. No distinct shoulder is observed on the long-wavelength side of the absorption maximum, suggesting that P3TODT is noncrystalline.

Grazing incidence X-ray diffraction (GIXRD) was performed on 100 nm thick films of P3HT-*b*-P3TODT, P3HT, and P3TODT prepared by spin coating from chlorobenzene solution at room temperature followed by annealing at 150 °C for 30 min. The GIXRD image of P3TODT (Figure 1f) shows a faint and very broad ring at around 4 Å. Consequently, the corresponding out-of-plane scattering plot (Figure 1b) reveals only a broad feature arising from the amorphous halo. This result is consistent with the much weaker peak intensity (at around 610 nm) observed for P3TODT thin films in the UV−vis spectrum. The GIXRD data for the P3HT-*b*-P3TODT and P3HT (Figure 1b, d, e) indicate a crystalline lamellar morphology. The peak at $2\theta = 5.6°$ corresponds to an interlayer *d*-spacing of 16.4 Å, and the other two diffraction peaks at $2\theta \sim 11.2°$ and $2\theta \sim 15.8°$ represent second and third-order reflections of the lamellae. These values are close to those reported for P3HT thin films[57] and indicate that alkyl side chains of P3HT are oriented vertical to the substrate to form an edge-on orientation, while the intermolecular $\pi-\pi$ stacking between the thiophene rings is parallel to the substrate.

Atomic force microscopy (AFM) images of the thin films of the P3HT-*b*-P3TODT (Figure 2a) reveal a periodic nanostructure with some degree of long-range order. The spacing of the nanostructures is approximately 20 nm. From the above results, including the AFM phase images and GIXRD profiles, we propose the ordered structure of P3HT-*b*-P3TODT films schematically shown in Figure 1c. After thermal annealing, the P3HT and P3TODT blocks separated from each other to self-assemble into lamellar morphology in the AFM phase images. Crystalline P3HT polymer chains showed an ordered molecular packing with their alkyl side chains aligned normal to the substrate in the thin films shown as the green domain in Figure 1c. On the other hand, P3TODT blocks segregated to form amorphous domains shown as the blue domain in Figure 1c.

It is well established that the morphology of diblock copolymers containing crystallizable blocks is influenced by both microphase segregation and segment crystallization.[32,31] It is also well-known that, under certain conditions, P3HT can crystallize into uniform crystalline lamellae. Therefore, the lamellar structure evident in the AFM analyses could result from either microphase separation of the dibock copolymer followed by crystallization or crystallization of the P3HT without microphase separation. We do not have conclusive evidence for the dominance of either mechanism, and elements of each could be at play. Reports suggest that crystallization of P3HT plays a dominant role in determining lamellar morphologies in BCP systems that contain high molecular weight P3HT.[31,58] One indication that microphase segregation plays a role in our system, as discussed later, is an increase in segregation strength observed upon the addition of bis-PCBA to P3HT-*b*-P3TODT. We also note that thin films of P3HT-*b*-P3TODT prepared by spin coating from 20 mg/mL chlorobenzene exhibit a the periodic morphology while the P3HT homopolymer with a similar molecular weight to that of

dx.doi.org/10.1021/cm203706h | *Chem. Mater.* 2012, 24, 622–632

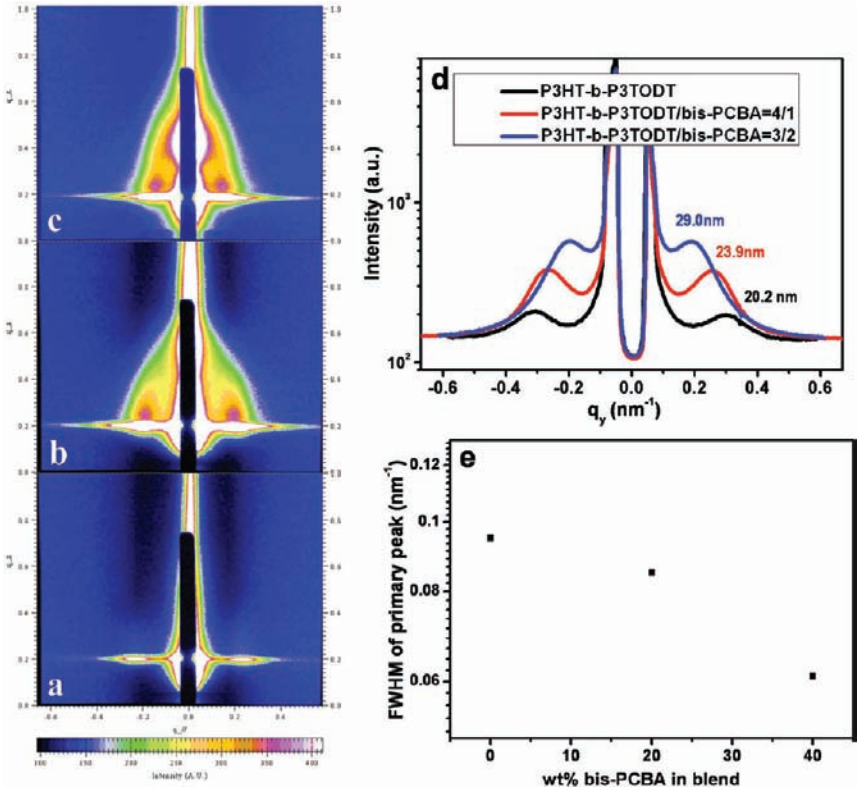

Figure 3. 2D GISAXS scattering profiles of the thin films of (a) P3HT-*b*-P3TODT, (b) P3HT-*b*-P3TODT/bis-PCBA (4/1), and (c) P3HT-*b*-P3TODT/bis-PCBA (3/2) after thermal annealing at 150 °C for 30 min. (d) Intensity profiles plotted against lateral momentum transfer vector q_y for three different GISAXS patterns shown in parts a–c. The *d*-spacing is 20.2 nm, 23.9 nm, and 29.0 nm, respectively. (e) Full width at half-maximum (fwhm) of the primary scattering peaks for blends with different bis-PCBA concentrations.

the P3HT block in P3HT-*b*-P3TODT processed under the same conditions does not show periodic nanoscale domains (Figure S2 in the Supporting Information). This difference suggests that the pattern shown in AFM results from BCP phase separation. Nevertheless, the evidence for microphase separation is not conclusive.

Morphology Characterization of P3HT-*b*-P3TODT/bis-PCBA Blends. The acid-functionalized fullerene, bis-PCBA, was chosen as the electron acceptor material due to its ability to hydrogen bond with the oligo(ethylene oxide) side chains of the P3TODT segments of the copolymer. The addition of a third component such as a nanoparticle or fullerene to a well ordered block copolymer can result in disorder or macrophase separation for the system due to the entropic penalty associated with chain stretching of the segments to accommodate the additive. We demonstrated that hydrogen bond interactions between the additives and a single block can not only overcome this penalty but can also increase the strength of phase segregation.[46] Parts b and c of Figure 2 show AFM phase images of the P3HT-b-P3TODT/bis-PCBA blend with different loadings of bis-PCBA after annealing at 150 °C for 30 min. At 20 wt % loading of bis-PCBA, the system still exhibits lamellar morphology. The images suggest that, upon increasing the concentration of bis-PCBA to 40 wt %, this system may be approaching an order-to-order transition from a lamellar to cylindrical morphology, although this is not confirmed by our analysis. TEM images in Figure 2e also show that the periodic nanostructure is maintained with bis-PCBA loading up to 40 wt %. We note that P3HT and P3TODT have similar electron densities and, thus, the contrast observed in TEM in the absence of staining is a clear indication that bis-PCBA selectively segregates to the P3TOT domain.

GISAXS was used to obtain statistically averaged information on the internal structure of these blends. The 2D-scattering profiles of a 100 nm thick film of P3HT-b-P3TODT and its blend are shown in Figure 3 a–c. The scattering profiles contain two prominent asymmetric features that are indicative of morphology oriented normal to the film surface. The position of the scattering maxima with respect to the q_{xy} axis, the scattering wave vector parallel to the surface of the film, corresponds to the average *d*-spacing ($d_{spacing} = 2\pi/q_{xy}$) in the *xy* plane of the film surface. The 1-D intensity profiles of the P3HT-*b*-P3TODT copolymer thin film, the blend with 20 wt % of bis-PCBA, and the blend with 40 wt % of bis-PCBA are plotted in Figure 3d versus the in-plane scattering vector. The scattering profiles show that as the loading of the bis-PCBA increases, the vertical streaks in the GISAXS patterns move to lower q_{xy} and the corresponding *d*-spacings progressively increase from 20.2 to 23.9 to 29.0 nm. The dependence of *d*-spacing on the blend ratio is strong evidence that the bis-PCBA derivative is incorporated in P3HT-*b*-P3TODT, as this result is inconsistent with macro-phase separation. Furthermore, there is an intensity enhancement in the composites compared to the neat block copolymer film. The intensity increase in the composite films relative to the neat P3HT-*b*-P3TODT film is expected, because the electron density contrast is enhanced when the bis-PCBA is incorporated in the blend film. No higher order reflections, as are commonly observed for strongly segregated coil–coil or rod–coil BCPs, are present. The rigid rod–rod structure in our system may preclude the formation of

dx.doi.org/10.1021/cm203706h | *Chem. Mater.* 2012, 24, 622–632

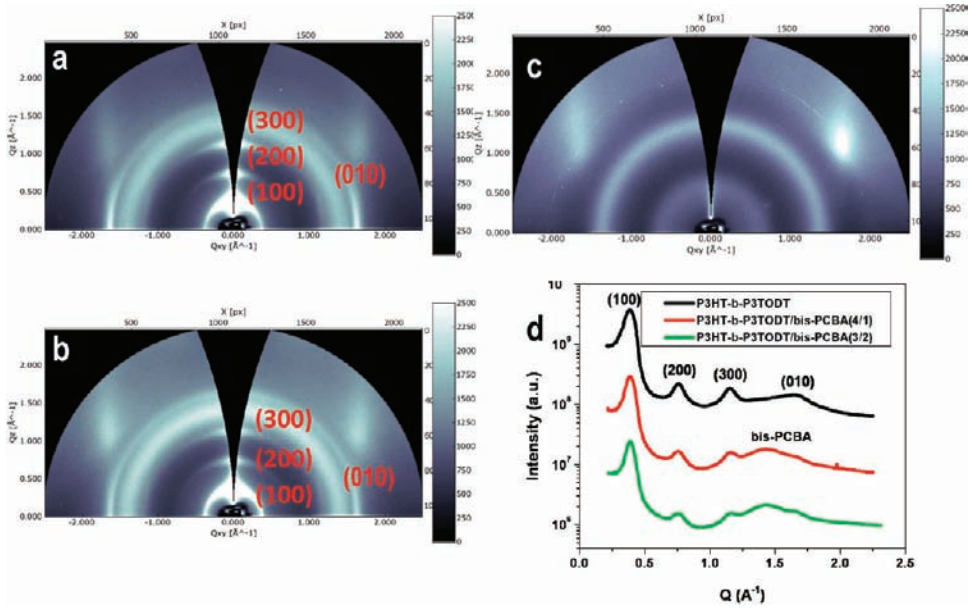

Figure 4. 2D GIXRD images of (a) P3HT-*b*-P3TODT/bis-PCBA (4/1), (b) P3HT-*b*-P3TODT/bis-PCBA (3/2), and (c) bis-PCBA films after annealing at 150 °C for 30 min: (d) overlay of GIXRD out-of-plane diffractograms of P3HT-*b*-P3TODT and its blends with different ratio of bis-PCBA.

well-defined domains with long-range order and the small electron density difference between the P3HT and P3TODT blocks may also contribute the absence measurable higher order peaks.

The GISAXS analysis provides insight into the roles of microphase segregation versus crystallization in the development of morphology in our systems. The relatively uniform spacing of crystalline lamellae observed in P3HT homopolymer can result broad and weak peaks in GISAXS scattering patterns.[15,59] By contrast, the scattering patterns of P3HT-b-P3TODT are more intense and sharper than those of P3HT homopolymer. Comparison of the full width at half-maximum (fwhm) of the primary peaks of the GISAXS profiles provides a comparison of the degree of order in BCP systems.[60,61] Smaller fwhm corresponds to a higher degree of segregation and overall order. Figure 3e compares the fwhm of the primary scattering peaks of P3HT-b-P3TODT and its blends with PCBA. Gaussian curve fitting results indicate that the fwhm value for blends with 40% PCBA (0.061 nm^{-1}) is significantly smaller than that of the neat P3HT-b-P3TODT (0.093 nm^{-1}). The smaller fwhm corresponds to a higher degree of spatial correlation, which, in turn, indicates an increase in segregation strength and stronger order in the material upon addition of the functionalized fullerene. The narrowing of the scattering patterns due to increased segregation strength upon addition of the functionalized fullerene is consistent with the behavior of other systems that exhibit additive driven assembly that we have reported.[46,62]

To investigate the effect of bis-PCBA loading on the crystallinity and molecular packing of P3HT-b-P3TODT in the blend films, GIXRD experiments were conducted on the same samples that were characterized by AFM and GISAXS; the diffraction images are shown in Figure 4. The diffractograms of neat bis-PCBA films show a broad peak at a lattice size of 14.1 Å, indicating no apparent orientation with respect to the surface of poorly ordered, nearly amorphous grains (Figure 4c). By comparison to Figure 1, besides the aforementioned broad ring, the diffraction image of the composite P3HT-b-P3TODT/bis-PCBA film is nearly identical to that of the P3HT-*b*-P3TODT thin films, i.e. the peaks that were attributed to ordered P3HT microdomains in neat P3HT-*b*-P3TODT thin films appear unchanged. This suggests that the bis-PCBA incorporation occurs primarily, if not exclusively, in the amorphous P3TODT domains.

The Influence of H-Bonding on Morphology and Fullerene Distribution. To determine if strong interactions between the block copolymer and fullerene derivatives facilitate the formation of a well-dispersed polymer-fullerene nanohybrid, a control experiment was carried out. Bis-PCBM, a fullerene derivative without strong interaction with the BCP, was blended with P3HT-*b*-P3TODT at 40 wt % loading. No primary peak was observed by GISAXS results (see Figure S3 in the Supporting Information), and the AFM images showed macrophase separation of bis-PCBM from the P3HT-*b*-P3TODT resulting in the formation of disorderd bis-PCBM domains on the order of 100 nm (see Figure S4 in the Supporting Information). Comparing the TEM images in Figure 2, it is apparent that macrophase separation occurs in the P3HT-*b*-P3TODT/bis-PCBM film (Figure 2d), while the P3HT-*b*-P3TODT/bis-PCBA system exhibits nanostructure morphology (Figure 2e). This illustrates the importance of the favorable interaction through hydrogen bonding. We employed FTIR to verify the specific interactions between bis-PCBA and oligo(ethylene oxide) side chain segments because of this method's sensitivity to hydrogen bond formation. Figure 5 shows infrared spectra for pure bis-PCBA, P3HT-*b*-P3TODT, and their blend. The monomodal peak centered at 1698 cm^{-1}, which is characteristic of the C=O stretching mode of the carboxylic acid dimer in bis-PCBA, is clearly split into two bands centered at 1730 cm^{-1} and 1704 cm^{-1} in the blend. The shoulder in the vicinity of 1730 cm^{-1} is attributable to the COOH bonded to ether, indicating the carboxylic acid−ether oxygen interaction, according to the reported literature.[63] When bis-PCBM is blended with P3HT-*b*-P3TODT, there is no evidence for this shift (Figure S5 in the Supporting Information). To further confirm that it is more

dx.doi.org/10.1021/cm203706h | *Chem. Mater.* 2012, 24, 622−632

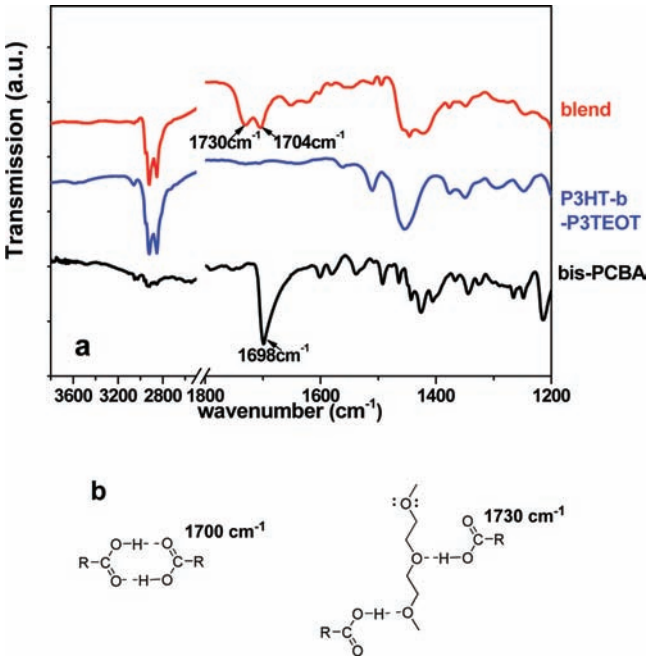

Figure 5. (a) FTIR spectra of bis-PCBA, P3HT-b-P3TODT, and their blend with the ratio of P3HT-*b*-P3TODT/bis-PCBA (3/2), respectively (from bottom to top). The split of the carbonyl group of COOH indicated the existence of H-bonding in the blend, and the peak at 1730 cm^{-1} is attributable to the COOH bonded to ether group. (b) Schematic diagram illustrating the carboxylic acid−ether oxygen interaction.

favorable for bis-PCBA to disperse in P3TODT domains than P3HT amorphous phase, the FTIR spectra of P3HT/bis-PCBA blend is shown as Figure S6 in the Supporting Information, where the peak for carbonyl stretching of the COOH group did not shift or spilt into two peaks, which is consistent with the absence of interaction between P3HT and bis-PCBA.

It has been previously reported[8−12] that prolonged thermal treatment induces the formation of large aggregates of PCBM in P3HT/PCBM films and degrades device performance. We studied the thin film morphologies of three different systems under harsh annealing conditions at 150 °C, using optical microscopy. It was clearly observed that large aggregates of PCBM appeared throughout the P3HT/PCBM films after annealing for 2 h, and after about 6 h of continued annealing, they grew to needle-like crystals, tens of micrometers in length (Figure 6a, b). Similar phenomena have been previously reported in the literature.[8−12] For the P3HT-*b*-P3TODT/bis-PCBM films (shown in Figure 6c, d), bis-PCBM crystallites also form, though the smaller in size than in those of P3HT/PCBM. In contrast, in the case of P3HT-*b*-P3TODT/bis-PCBA (as shown in Figure 6e, f), only a small number of small bis-PCBA crystals was observed, even after 6 h of annealing. This suggests that the formation of fullerene aggregates is suppressed by the reduced translational mobility of the fullerene derivatives that are strongly associated with the polymer chains by hydrogen bonding. To suppress the PCBM aggregation, Gaudiana and co-workers synthesized cross-linkable fullerene derivatives containing epoxy or glycidyl functionality.[3,64] They succeeded in suppressing the large aggregation of the fullerene derivative under thermal annealing after acid-catalyzed cross-linking. Morphological stabilization of polymer thin films has also been examined using thermal or photo-cross-linkable polythiophenes by chemical modification.[10,12,65] In our approach, these goals are accomplished by simple blending of two components that can hydrogen bond with one another.

Device Performance of P3HT-*b*-P3TODT/bis-PCBA Blends. Bottom gate, top contact field-effect transistors were prepared by the contact film transfer method[66] to investigate the charge carrier mobility of these block copolythiophene materials. The devices exhibited typical p-type behavior as shown by the transfer and output curves in Figure S7 in the Supporting Information. A clear field effect is observed from the output characteristics, and the hole mobility was estimated as 0.10 $cm^2\ V^{-1}\ s^{-1}$ from the transfer characteristics in the saturation regime (V_{ds} = −80 V). This value is slightly lower than that of P3HT homopolymer prepared under the same conditions, which exhibits a hole mobility value of 0.19 $cm^2\ V^{-1}s^{-1}$. This difference may be due to the amorphous P3TODT in the block copolymer, which reduces the crystalline content of the polymer compared to homo-P3HT. It is known that an ordered crystalline structure is favorable for charge carrier transport and high mobility of conjugated polymers.[67] Nonetheless, previous studies[68] on P3HT based block copolymer by using contact film transfer also showed a similar mobility value of 0.10 $cm^2\ V^{-1}s^{-1}$, which is in-line with our measurement.

The blends of P3HT-*b*-P3TODT with bis-PCBA or bis-PCBM were incorporated into BHJ OPVs as active layers with

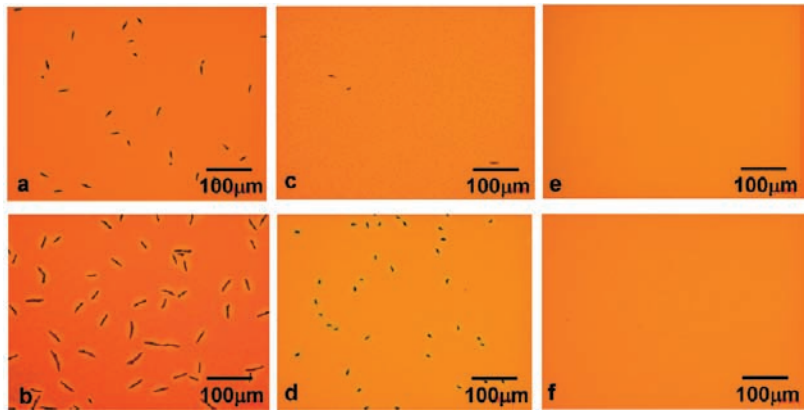

Figure 6. Optical micrographs of (a, b) P3HT/PCBM (3/2), (c, d) P3HT-*b*-P3TODT/bis-PCBM (3/2), and (e, f) P3HT-b-P3TODT/bis-PCBA (3/2) during thermal annealing at 150 °C on the device. The annealing time for a, c, and e is 2 h, and that for b, d, and f is 6 h.

dx.doi.org/10.1021/cm203706h | *Chem. Mater.* 2012, 24, 622−632

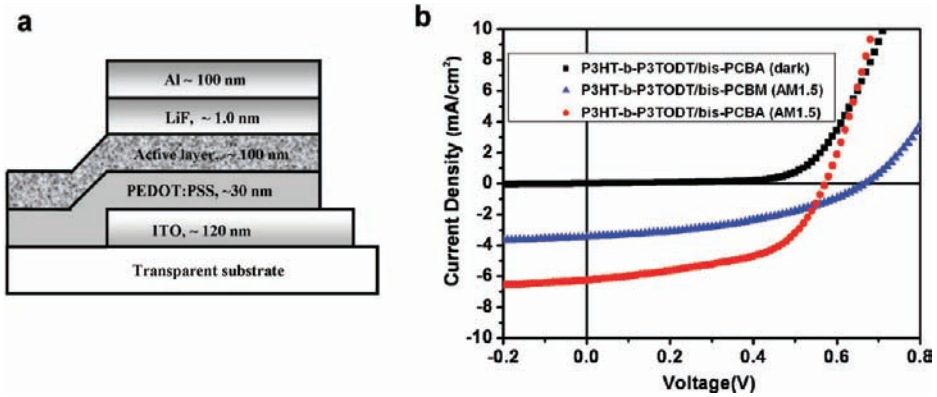

Figure 7. (a) Schematic representation of the OPV device architecture. (b) Current−voltage curves of the solar cells with an active layer of P3HT-*b*-P3TODT/bis-PCBM (3/2) (blue ▲) and P3HT-*b*-P3TODT/bis-PCBA (3/2) (red ●) under AM 1.5 (100 mW/cm^2) illumination. Measurements were done after annealing at 150 °C for 10 min.

a device architecture of ITO/PEDOT:PSS/active layer/LiF/Al on glass substrates (Figure 7a). As seen from the device performance (Figure 7b and Table S1 in the Supporting Information), the P3HT-*b*-P3TODT/bis-PCBA system exhibits a higher J_{sc} and a higher fill factor (FF) and, consequently, a higher PCE, in comparison to those with the P3HT-*b*-P3TODT/bis-PCBM system. For the P3HT-*b*-P3TODT/bis-PCBM system, large domains of bis-PCBM, up to 50−100 nm, reduce the interfacial area available for charge separation and result in low-efficiency devices. Evidently, the ability to incorporate bis-PCBA into a single domain that has a similar length as the exciton diffusion length has been proven to be advantageous in this instance. We note that although the P3HT-*b*-P3TODT/bis-PCBA gave good initial device performance, which enables us to evaluate the long-term thermal stability of the devices in the following sections, its PCE number is still below that of the P3HT/PCBM model devices we tested (Table S1 in the Supporting Information). There maybe a number of reasons for this difference including processing issues, moisture uptake in the oligo(ethylene oxide) side chains and interfacial issues between active layers and electrodes.

We studied the influence of processing conditions on the PCE of P3HT-*b*-P3TODT/bis-PCBA devices and found that efficiency of the as-spun devices remained nearly constant after preannealing and postannealing (Table 1). This suggests that

Table 1. Device Performance of Solar Cells under Different Processing Conditions[a]

	V_{oc} (V)	FF (%)	J_{sc} (mA/cm^2)	PCE (%)
as spun	0.56	52.46	6.34	1.86
preanneal.	0.57	53.75	6.35	1.95
postanneal.	0.58	55.67	6.32	2.04

[a]P3HT-*b*-P3TODT/bis-PCBA = 3/2 (by wt). Film thickness is about 100 nm. Measurement was conducted under irradiation of AM1.5 (100 mW/cm^2).

the spontaneous formation of lamellar domains (characterized above) occurs immediately after spin-casting without any need for solvent or thermal annealing. Furthermore, the morphology formed is sufficiently stable, such that the PCE is not sensitive to processing conditions. This could be an advantage over the P3HT/PCBM system, where the efficiency is largely dependent on the processing and annealing conditions.

That hydrogen bonding interactions promote morphological stability under extended annealing should enhance thermal and aging stability of the device. To assess this point, BHJ devices composed of P3HT-*b*-P3TODT/bis-PCBA and P3HT/PCBM were fabricated side-by side and were subsequently annealed at 150 °C in a glovebox filled with Ar as an accelerated aging test for device stability. Figure 8 compares the PCE of these two

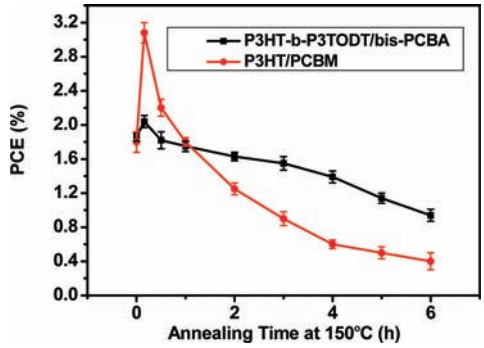

Figure 8. PCE as a function of annealing time for the P3HT/PCBM (3/2) (red ●) and P3HT-*b*-P3TODT/bis-PCBA (3/2) (black ■) devices, the SD is calculated by the average number of six devices.

systems as a function of annealing time. Both devices showed similar average initial PCEs of ca. 2%. In the course of the thermal annealing, the PCE for P3HT/PCBM increased dramatically for the first 10 min, and then, they gradually decreased to 0.4% after annealing for 6 h. In contrast, the rate of degradation for P3HT-*b*-P3TODT is much lower, and the PCE remained above 1.0% after annealing for 6 h. As shown in the previous section, the limited crystallization of bis-PCBA resulted from hydrogen bonding suppresses the deterioration of PCE. However, the device stability result, while significantly improved, is not optimum. There might be other factors that contribute to the degradation at play, such as interfacial degradation. Further studies to resolve these issues are currently in progress.

■ CONCLUSIONS

We have shown that the cooperative self-assembly of conjugated diblock copolythiophene P3HT-*b*-P3TODT and COOH-functionalized bis-PCBA fullerenes yields photovoltaic devices with well-defined structures and improved morpho-

dx.doi.org/10.1021/cm203706h | *Chem. Mater.* 2012, 24, 622−632

logical stability. The strong interactions between bis-PCBA and the oligo(ethylene oxide) side chain result in a preferential distribution of the fullerenes within the P3TODT domains and lead to nanostructured D/A interpenetrated networks. GISAXS results, in combination with AFM and TEM images, indicate that there is lamellar morphology of the blend system with 40 wt % loading of bis-PCBA on the 10−20 nm domain size. Moreover, the P3HT-*b*-P3TODT/bis-PCBA blend was stable for extended periods of time at elevated annealing temperatures (150 °C) without evidence of the fullerene aggregation or crystallization. In comparison, annealing blends of the block copolymer and bis-PCBM, which does not interact strongly with the oligo(ethylene oxide) side chains, leads to aggregation of the fullerene. Photovoltaic devices prepared from these stabilized layers exhibited 2.04% power conversion efficiencies, which decreased to 0.95% over 6 h annealing at 150 °C, whereas typical P3HT/PCBM devices, displaying a 3.08% PCE, degraded to 0.4% PCE over the same period. Overall, the incorporation of hydrogen bonding units in the photoactive layer has led to improved photovoltaic performance as a result of enhanced morphological control of the BHJ. This method provides a general approach to obtain reliable donor/acceptor morphologies by cooperative assembly facilitated by strong component interactions and to achieve efficient photovoltaic devices with enhanced thermal stability.

■ ASSOCIATED CONTENT

Supporting Information

Experimental details, additional figures showing the ^{1}H NMR, GPC, FTIR, GIXRD, GISAXS, and AFM of the polymers and the blends. This material is available free of charge via the Internet at http://pubs.acs.org.

■ AUTHOR INFORMATION

Corresponding Author

*E-mail: watkins@polysci.umass.edu.

Notes

The authors declare no competing financial interest.

■ ACKNOWLEDGMENTS

Funding from the NSF Center for Hierarchical Manufacturing (CMMI-0531171) supported studies on the morphology of blends with strongly interacting components. Funding from the Department of Energy supported Energy Frontier Research Center at the University of Massachusetts (DOE DE-PS02-08ER15944) supported the photovoltaic device fabrication, characterization, and testing and is gratefully acknowledged. GISAXS measurement was done at the Cornell High Energy Synchrotron Source (CHESS), a national user facility supported by the National Science Foundation and the National Institutes of Health/National Institute of General Medical Sciences under Award No. DMR-0225180. GIXRD measurement was done at Stanford Synchrotron Radiation Lightsource (SSRL), operated by the Department of Energy.

■ REFERENCES

(1) Sariciftci, N. S.; Smilowitz, L.; Heeger, A. J.; Wudl, F. *Science* **1992**, *258*, 1474.
(2) Gunes, S.; Neugebauer, H.; Sariciftci, N. S. *Chem. Rev.* **2007**, *107*, 1324.
(3) Zhu, Z.; Hadjikyriacou, S.; Waller, D.; Gaudiana, R. *J. Macromol. Sci., Part A: Pure Appl. Chem.* **2004**, *A41*, 1467.
(4) Ma, W.; Yang, C.; Gong, X.; Lee, K.; Heeger, A. J. *Adv. Funct. Mater.* **2005**, *15*, 1617.
(5) Kim, Y.; Cook, S.; Tuladhar, S. M.; Choulis, S. A.; Nelson, J.; Durrant, J. R.; Bradley, D. D. C.; Giles, M.; McCulloch, I.; Ha, C.-S.; Ree, M. *Nat. Mater.* **2006**, *5*, 197.
(6) Li, G.; Shrotriya, V.; Yao, Y.; Huang, J. S.; Yang, Y. *J. Mater. Chem.* **2007**, *17*, 3126.
(7) Campoy-Quiles, M.; Ferenczi, T.; Agostinelli, T.; Etchegoin, P. G.; Kim, Y.; Anthopoulos, T. D.; Stavrinou, P. N.; Bradley, D. D. C.; Nelson, J. *Nat. Mater.* **2008**, *7*, 158.
(8) Bertho, S.; Janssen, G.; Cleij, T. J.; Conings, B.; Moons, W.; Gadisa, A.; D'Haen, J.; Goovaerts, E.; Lutsen, L.; Manca, J.; Vanderzande, D. *Sol. Energy Mater. Sol. Cells* **2008**, *92*, 753.
(9) Sivula, K.; Luscombe, C. K.; Thompson, B. C.; Fréchet, J. M. J. *J. Am. Chem. Soc.* **2006**, *128*, 13988.
(10) Gholamkhass, B.; Holdcroft, S. *Chem. Mater.* **2010**, *22*, 5371.
(11) Lee, J. U.; Jung, J. W.; Emrick, T.; Russell, T. P.; Jo, W. H. *Nanotechnology* **2010**, *21*, 105201.
(12) Miyanishi, S.; Tajima, K.; Hashimoto, K. *Macromolecules* **2009**, *42*, 1610.
(13) Pettersson, L. A. A.; Roman, L. S.; Inganas, O. *J. Appl. Phys.* **1999**, *86*, 487.
(14) Halls, J. J. M.; Pichler, K.; Friend, R. H.; Moratti, S. C.; Holmes, A. B. *Appl. Phys. Lett.* **1996**, *68*, 3120.
(15) Chen, D.; Liu, F.; Wang, C.; Nakahara, A.; Russell, T. P. *Nano Lett.* **2011**, *11*, 2071.
(16) Chirvase, D.; Parisi, J.; Hummelen, J. C.; Dyakonov, V. *Nanotechnology* **2004**, *15*, 1317.
(17) Nguyen, L. H.; Hoppe, H.; Erb, T.; Gunes, S.; Gobsch, G.; Sariciftci, N. S. *Adv. Funct. Mater.* **2007**, *17*, 1071.
(18) Zhao, Y.; Xie, Z. Y.; Qu, Y.; Geng, Y. H.; Wang, L. X. *Appl. Phys. Lett.* **2007**, *90*, 043504.
(19) Peet, J.; Kim, J. Y.; Coates, N. E.; Ma, W. L.; Moses, D.; Heeger, A. J.; Bazan, G. C. *Nat. Mater.* **2007**, *6*, 497.
(20) Janssen, G.; Aguirre, A.; Goovaerts, E.; Vanlaeke, P.; Poortmans, J.; Manca, J. *Eur. Phys. J.: Appl. Phys.* **2007**, *37*, 287.
(21) Leibler, L. *Macromolecules* **1980**, *13*, 1602.
(22) Bates, F. S.; Fredrickson, G. H. *Phys. Today* **1999**, *52*, 32.
(23) Hadziioannou, G. *MRS Bull.* **2002**, *27*, 456.
(24) Botiz, I.; Darling, S. B. *Mater. Today* **2010**, *13*, 42.
(25) Darling, S. *Prog. Polym. Sci.* **2007**, *32*, 1152.
(26) Segalman, R. A.; McCulloch, B.; Kirmayer, S.; Urban, J. J. *Macromolecules* **2009**, *42*, 9205.
(27) Topham, P. D.; Parnell, A. J.; Hiorns, R. C. *J. Polym. Sci., Part B: Polym. Phys.* **2011**, *49*, 1131.
(28) Yu, X.; Xiao, K.; Chen, J.; Lavrik, N. V.; Hong, K.; Sumpter, B. G.; Geohegan, D. B. *ACS Nano* **2011**, *5*, 3559.
(29) Dai, C.-A.; Yen, W.-C.; Lee, Y.-H.; Ho, C.-C.; Su, W.-F. *J. Am. Chem. Soc.* **2007**, *129*, 11036.
(30) Botiz, I.; Darling, S. B. *Macromolecules* **2009**, *42*, 8211.
(31) Ho, V.; Boudouris, B. W.; McCulloch, B. L.; Shuttle, C. G.; Burkhardt, M.; Chabinyc, M. L.; Segalman, R. A. *J. Am. Chem. Soc.* **2011**, *133*, 9270.
(32) Boudouris, B. W.; Frisbie, C. D.; Hillmyer, M. A. *Macromolecules* **2010**, *43*, 3566.
(33) Stalmach, U.; de Boer, B.; Videlot, C.; van Hutten, P. F.; Hadziioannou, G. *J. Am. Chem. Soc.* **2000**, *122*, 5464.
(34) Yang, C.; Lee, J. K.; Heeger, A. J.; Wudl, F. *J. Mater. Chem.* **2009**, *19*, 5416.
(35) Dante, M.; Yang, C.; Walker, B.; Wudl, F.; Nguyen, T.-Q. *Adv. Mater.* **2010**, *22*, 1835.
(36) Bu, L.; Guo, X.; Yu, B.; Qu, Y.; Xie, Z.; Yan, D.; Geng, Y.; Wang, F. *J. Am. Chem. Soc.* **2009**, *131*, 13242.
(37) Miyanishi, S.; Zhang, Y.; Tajima, K.; Hashimoto, K. *Chem. Commun.* **2010**, *46*, 6723.
(38) Osaka, I.; McCullough, R. D. *Acc. Chem. Res.* **2008**, *41*, 1202.
(39) Yokozawa, T.; Yokoyama, A. *Chem. Rev.* **2009**, *109*, 5595.
(40) Verduzco, R.; Botiz, I.; Pickel, D. L.; Kilbey, S. M.; Hong, K.; Dimasi, E.; Darling, S. B. *Macromolecules* **2011**, *44*, 530.

(41) Ren, G. Q.; Wu, P. T.; Jenekhe, S. A. *Chem. Mater.* **2010**, *22*, 2020.
(42) Zhang, Y.; Tajima, K.; Hirota, K.; Hashimoto, K. *J. Am. Chem. Soc.* **2008**, *130*, 7812.
(43) Zhang, Y.; Tajima, K.; Hashimoto, K. *Macromolecules* **2009**, *42*, 7008.
(44) He, M.; Zhao, L.; Wang, J.; Han, W.; Yang, Y.; Qiu, F.; Lin, Z. *ACS Nano* **2010**, *4*, 3241.
(45) Lee, E.; Hammer, B.; Kim, J.-K.; Page, Z.; Emrick, T.; Hayward, R. C. *J. Am. Chem. Soc.* **2011**, *133*, 10390.
(46) Lin, Y.; Daga, V. K.; Anderson, E. R.; Gido, S. P.; Watkins, J. J. *J. Am. Chem. Soc.* **2011**, *133*, 6513.
(47) Sary, N.; Richard, F.; Brochon, C.; Leclerc, N.; Leveque, P.; Audinot, J. N.; Berson, S.; Heiser, T.; Hadziioannou, G.; Mezzenga, R. *Adv. Mater.* **2010**, *22*, 763.
(48) Worfolk, B. J.; Rider, D. A.; Elias, A. L.; Thomas, M.; Harris, K. D.; Buriak, J. M. *Adv. Funct. Mater.* **2011**, *21*, 1816.
(49) MacLeod, J. M.; Ivasenko, O.; Fu, C.; Taerum, T.; Rosei, F.; Perepichka, D. F. *J. Am. Chem. Soc.* **2009**, *131*, 16844.
(50) Kira, A.; Tanaka, M.; Umeyama, T.; Matano, Y.; Yoshimoto, N.; Zhang, Y.; Ye, S.; Lehtivuori, H.; Tkachenko, N. V.; Lemmetyinen, H.; Imahori, H. *J. Phys. Chem. C* **2007**, *111*, 13618.
(51) Huang, C.-H.; McClenaghan, N. D.; Kuhn, A.; Bravic, G.; Bassani, D. M. *Tetrahedron* **2006**, *62*, 2050.
(52) Huang, C.-H.; McClenaghan, N. D.; Kuhn, A.; Hofstraat, J. W.; Bassani, D. M. *Org. Lett.* **2005**, *7*, 3409.
(53) Qian, G.; Wang, Z. Y. *Can. J. Chem.* **2010**, *88*, 192.
(54) Yokozawa, T.; Adachi, I.; Miyakoshi, R.; Yokoyama, A. *High Perform. Polym.* **2007**, *19*, 684.
(55) Mannsfeld, S. C. B.; Tang, M. L.; Bao, Z. *Adv. Mater.* **2011**, *23*, 127.
(56) Brown, P. J.; Thomas, D. S.; Köhler, A.; Wilson, J. S.; Kim, J.-S.; Ramsdale, C. M.; Sirringhaus, H.; Friend, R. H. *Phys. Rev. B* **2003**, *67*, 064203.
(57) Chen, T.-A.; Wu, X.; Rieke, R. D. *J. Am. Chem. Soc.* **1995**, *117*, 233.
(58) Ho, V.; Boudouris, B. W.; Segalman, R. A. *Macromolecules* **2010**, *43*, 7895.
(59) Zhang, R.; Li, B.; Iovu, M. C.; Jeffries-El, M.; Sauvé, G.; Cooper, J.; Jia, S.; Tristram-Nagle, S.; Smilgies, D. M.; Lambeth, D. N.; McCullough, R. D.; Kowalewski, T. *J. Am. Chem. Soc.* **2006**, *128*, 3480.
(60) Tokarev, I.; Krenek, R.; Burkov, Y.; Schmeisser, D.; Sidorenko, A.; Minko, S.; Stamm, M. *Macromolecules* **2004**, *38*, 507.
(61) Tirumala, V. R.; Romang, A.; Agarwal, S.; Lin, E. K.; Watkins, J. J. *Adv. Mater.* **2008**, *20*, 1603.
(62) Daga, V. K.; Watkins, J. J. *Macromolecules* **2010**, *43*, 9990.
(63) Lee, J. Y.; Painter, P. C.; Coleman, M. M. *Macromolecules* **1988**, *21*, 346.
(64) Drees, M.; Hoppe, H.; Winder, C.; Neugebauer, H.; Sariciftci, N. S.; Schwinger, W.; Schaffler, F.; Topf, C.; Scharber, M. C.; Zhu, Z. G.; Gaudiana, R. *J. Mater. Chem.* **2005**, *15*, 5158.
(65) Griffini, G.; Douglas, J. D.; Piliego, C.; Holcombe, T. W.; Turri, S.; Fréchet, J. M. J.; Mynar, J. L. *Adv. Mater.* **2011**, *23*, 1660.
(66) Wei, Q.; Miyanishi, S.; Tajima, K.; Hashimoto, K. *ACS Appl. Mater. Interfaces* **2009**, *1*, 2660.
(67) Sirringhaus, H.; Brown, P. J.; Friend, R. H.; Nielsen, M. M.; Bechgaard, K.; Langeveld-Voss, B. M. W.; Spiering, A. J. H.; Janssen, R. A. J.; Meijer, E. W.; Herwig, P.; de Leeuw, D. M. *Nature* **1999**, *401*, 685.
(68) Zhang, Y.; Tajima, K.; Hashimoto, K. *Synth. Met.* **2011**, *161*, 225.